ISSN: 2664-9640

Research on stress model of thin-walled tube shell by ring vector extrusion

Xu Li, Hongjun Li, Xingzhang Li and Chi Zhang

Wuhan Textile University, Wuhan 430200, China

Abstract

Hollow thin-walled parts (electronic packaging shell, detonator shell, gun shell, etc.) which need a reduction diameter process in order to fix or seal the embedded parts. Establishing a plastic micro-element stress model for the annular vector reduction of the tube shell Based on the Barlat'96 yield criterion and M-K groove theory, combined with L.H. The influence of the geometry of the tube shell on the distribution of the elasto-plastic deformation region and the variation of the stresses in the necking zone are analysed. Simulati of the tube shell annular vector squeeze diameter process with the help of ANSYS finite element analysis software. The variation law of stress distribution in the thickness direction of inner wall and necking zone during annular vector extrusion of tube shell is analyzed. Finally, the accuracy of simulation results is verified by experiments.

Keywords

Tube shells; ring vector extrusion;necking forming; equivalent stress.

1. Introduction

The tube has the characteristic advantage of light weight, and parts with different diameters can be obtained through reducing forming, which is widely used in automobile transmission shaft tube, steering shaft, etc. [1-3]. In the 1970s, some scholars analyzed the coreless pushing and shrinking of tube shell [4-6]. Since then, many scholars have conducted a lot of research on incomplete linear forming, such as energy method proposed by cao[7], and ju[8] on tube bending forming. However, there are great limitations for the tube shell sagittal extrusion necking forming. The necking area is located in the die during the tube shell necking forming process, and the final forming state can be observed only after the forming is completed. In terms of numerical simulation of incomplete linear forming of tube and sheet metal, li[9-11] developed a prediction mold of thin-walled tube bending through finite element and energy principle. Liu[12] and others took thin-walled aluminum alloy tube as the research object, combined with the initial defects of thin-walled tube, predicted the plastic forming of elbow under different constraints.

According to the above-mentioned incomplete linear forming theory of thin-walled parts and the current situation of numerical simulation, the theory can analyze the cause law of necking forming, but only the combination of theoretical analysis, numerical simulation and experiment can better study the necking forming law of thin-walled tube shell by sagittal extrusion

2. Theoretical analysis of tube shell ring sagittal extrusion reduction

The schematic diagram of tube shell extrusion and diameter reduction is shown in Figure 1. Take the tube and shell axis as the axial coordinate axis X, the radial vector r as the radial coordinate axis, and the rotation angle θ Establish a cylindrical coordinate system for circumferential coordinates.

ISSN: 2664-9640

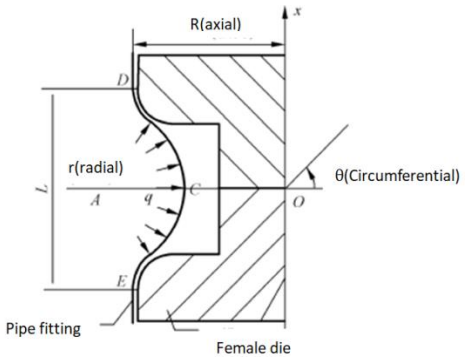

Figure 1: Schematic diagram of extrusion

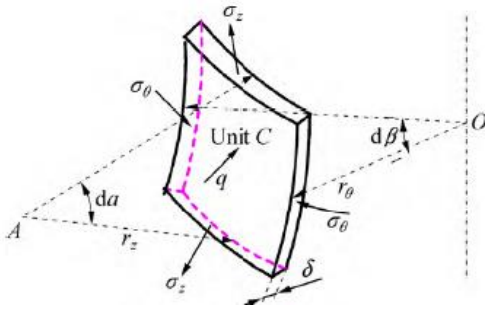

Figure 2: Force analysis of micro element

set up ω、u、v is the radial, axial and circumferential displacement of the micro element on the neutral surface of the tube shell, and it is assumed that the shape of the reduced diameter is cosine distribution. Then:

$$\begin{cases} u = u_n(x)cosn\theta \\ v = v_n(x)cosn\theta \\ \omega = \omega_n(x)cosn\theta \end{cases} \tag{1}$$

In the above formula, n is the circumferential wave number. In order to facilitate the solution, it is necessary to assume that D and E in Figure 1 are fixed boundary constraints. That is, when x=l/2, there are:

$$\omega = \mathrm{u} = \mathrm{v} = \partial\omega/\partial\mathrm{x} \tag{2}$$

$$\begin{cases} u_n(x) = \sum_{i=1}^{4}\left[\overline{u}_i A_i sh\left(r_i^{\frac{1}{2}}x\right) + \overline{u}_i B_i sh(r_i^{\frac{1}{2}}x)\right] \\ v_n(x) = \sum_{i=1}^{4}\left[\overline{v}_i A_i ch\left(r_i^{\frac{1}{2}}x\right) + \overline{v}_i B_i sh(r_i^{\frac{1}{2}}x)\right] \\ \omega_n(x) = \sum_{i=1}^{4}\left[A_i ch\left(r_i^{\frac{1}{2}}x\right) + B_i sh(r_i^{\frac{1}{2}}x)\right] \end{cases} \quad \begin{cases} \overline{u}_i = \frac{-r_i^{\frac{1}{2}}(n^2+\mu r_i)}{(r_i-n^2)^2} \\ \overline{v}_i = \frac{n[(2+\mu)r_i-n^2]}{(r_i-n^2)^2} \end{cases} \tag{3}$$

i = 1,2,3,4. r_i is the four roots of characteristic equation (4).

$$(\mathrm{r}-n^2)^4 + 12(1-\mu^2)\left(\frac{R}{L}\right)^2 \times \left[\frac{1}{2}r + n^2(r-n^2)^2\frac{q_{cr}}{E\delta} + r^2\right] = 0 \tag{4}$$

In the formula,δ Is the wall thickness of the pipe shell, and L is the reduced length.

Bringing the boundary condition (2) into equation (3) gives the equation for A_i and B_i of a system of 8 linear chi-squared algebraic equations. Then the reduced external pressure q_{cr} The analytical expression for：

$$\det(\mathrm{Z}, \beta, K_P, \mu) = 0 \tag{5}$$

Where Z is the Bathorf parameter, $\mathrm{Z} = \sqrt{1-\mu^2}\,\mathrm{L}^2/\mathrm{R}\delta$.β and K_p are the parameters related to the circumferential beam n and the reduced external pressure q_{cr} are the parameters related to the circumferential beam n and the scaled external pressure, and the expressions are：

$$k_p = \frac{q_{cr}RL^2}{\pi^2 D} \qquad \beta = (\frac{L}{\pi R})\mathrm{n} \tag{6}$$

In the formula, $\mathrm{D} = \mathrm{E}\delta^3/12(1-\mu^2)$ is the flexural stiffness of the tube shell when $\mathrm{Z} \geq 10$, that is $\mathrm{L} \geq \sqrt{10\mathrm{R}\delta}$ when $k_p = a_p Z^{1/2}$， $\beta = b_p Z^{1/4}$.Where a_p and b_p correspond to the coefficients of the power-only function, respectively, and $a_p \approx 1.51$， $b_p \approx 0.96$.When $\mathrm{Z} \leq 10$, $\mathrm{L} \leq \sqrt{10\mathrm{R}\delta}$ when there is $k_p = \exp 1.61$, the $\beta = \exp 0.18$. Taking the above expressions into (6) gives:

$$\frac{q_{cr}}{E} = 0.883a_p\sqrt{\left(\frac{\delta}{R}\right)^5}/(\frac{L}{R}) \qquad \mathrm{n} = 3.12b_p/\sqrt[4]{\left(\frac{L}{R}\right)^2\left(\frac{\delta}{R}\right)} \tag{7}$$

ISSN: 2664-9640

In order to make the above equation applicable to the global domain of values of the Bathorf parameter Z, it is specified that when $Z \leq 10$ When, again, there exist a_p and b_p, in order to satisfy β and k_p take on the values , there should be $a_p = e^{1.61}/Z^{1/2}$ and $b_p = e^{0.18}/Z^{1/4}$ .Equation (7) is only applicable to the elastic range, i.e. $q_{cr} \leq q_s$ when q_s for the tube shell yield external pressure, the initial did not produce plastic deformation when it can be considered that

$$q_s = \sigma_{\theta-s} - \delta/R = \sigma_s \delta/R\sqrt{1 - k_s + k_s^2} \tag{8}$$

Where $\sigma_{\theta-s}$ is the circumferential stress component at yield of the tube shell. k_s is the ratio of yield stress components.When $q_{cr} > q_s$, the tube shell undergoes plastic deformation, the geometric conditions for plastic deformation are:

$$(\delta/R)^{3/2}/(L/R) > \sigma_S/\left[0.883\sqrt{1 - k_s + k_s^2}a_p E\right] \tag{9}$$

The initial deformation state of the necking zone is circumferential $\sigma_\theta \leq 0$, axially$\sigma_z \geq 0$, as shown in Figure 2 for the forces on the micro element.

When satisfying equation (9), plastic deformation of the tube shell must occur. That is:

$$\begin{cases} \frac{(\delta/R)^{3/2}}{(L/R)} > 0.75\sigma_s/E & (L \geq \sqrt{10R\delta}) \\ \frac{(\delta/R)^2}{(L/R)^2} > 0.216\sigma_s/E & (L \leq \sqrt{10R\delta}) \end{cases} \tag{10}$$

If the thickness to neck ratio δ/R ratio remains constant, the wider the neck reduction area L/R the smaller the neck reduction area (if the neck reduction area width to diameter ratioL/Rremains constant, the greater the thickness to neck ratio δ/R), the further away from the elastic zone the reduction will be; conversely, the closer it will be to the elastic zone.

From the relevant equation in Elasticity and plasticity [13] , the stress-strain when deformation occurs is shown in equation (11).

$$\begin{cases} \sigma_{ij} = \left[L_{ijkl} - \left(\frac{a}{H+h}\right)\frac{\partial g}{\partial \varepsilon_{ij}}\frac{\partial g}{\partial \varepsilon_{kl}}\right]\varepsilon_{kl} \\ \varepsilon_{ij} = \left[M_{ijkl} + \left(\frac{a}{h}\right)\frac{\partial f}{\partial \sigma_{ij}}\frac{\partial f}{\partial \varepsilon_{kl}}\right]\sigma_{kl} \ (h \neq 0) \end{cases} \quad a = \begin{cases} 1, & (\text{in plastic loading}) \\ 0, & (\text{in the elastic state or during unloading}) \end{cases} \tag{11}$$

3. Finite element model analysis of circular vector extrusion of tube shell

3.1. The analysis of residual stress

The equivalent force cloud after the extrusion and compression of the tube shell body is shown in Figure 3 (the grey transparent part of the figure is the extruded body). From the outside of the tube shell, the stresses are distributed symmetrically in bands on both sides of the extruded part, and from the central axis of the tube shell, the stresses are distributed in a circular pattern, and the stresses decrease along the radial direction. The maximum residual equivalent force is 319.76 MPa, which is distributed on the inner surface of the extruded part.

In order to study the stress variation law of the micro elements in the necking area during the shrink forming process of the tube shell, the stress distribution variation of the inner wall surface and the thickness direction of the necking area of the tube shell is statistically and analytically analysed.

ISSN: 2664-9640

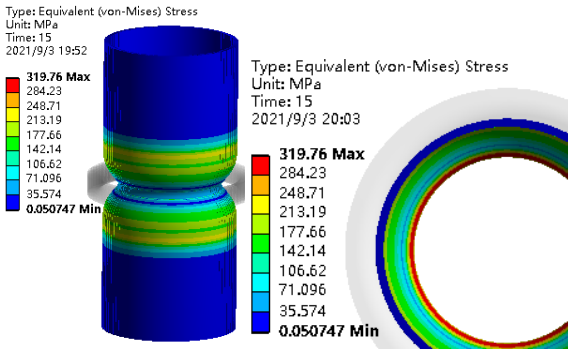

Figure 3: Equivalent stress nephogram

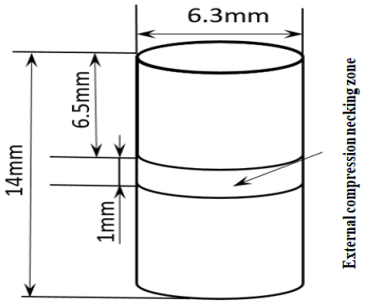

Figure 1 :Dimensions of thin-walled tube shell

The size parameters of each part of the thin-walled tube shell are shown in Figure 4, where the wall thickness is 0.2mm, the radius is R=3.15, and the width of the neck shrinkage area L is 1mm. The metal shell is made of Q235, Young modulus 210Gpa, Poisson ratio 0.274, yield strength 255Mpa, and tangent modulus 9420Mpa.

3.2. Analysis of stress changes on the inner wall surface

The stress changes on the inner wall surface during ring sagittal squeezing and compression of the diameter are shown in Figure 5. The overall equivalent force is a convex distribution with the neck shrinkage area as the apex, when the squeezing pressure is less than 435N (line 2), with the increase in squeezing pressure, the bump is getting higher and higher (i.e. the maximum equivalent force increases with the increase in squeezing pressure) when the shrinkage forming is in the elastic stage.

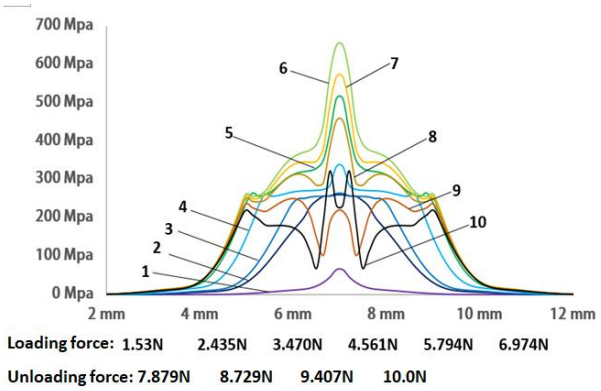

Figure 5: Stress variation of inner wall

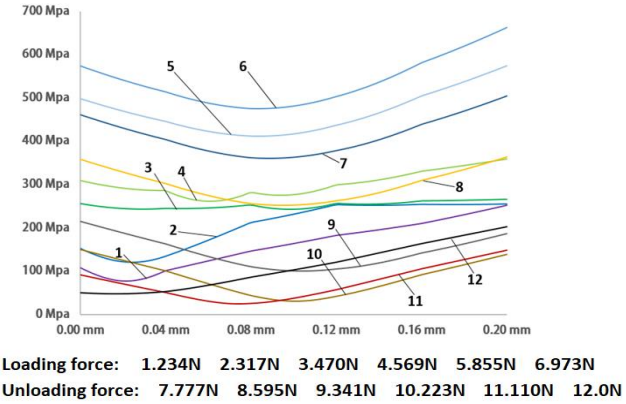

Figure 6: Stress variation in the direction of the wall

When the squeeze pressure is 435-470N (lines 2-3), the maximum equivalent force in the yield limit of 255Mpa or so almost no longer increases, but the stress reaches 255Mpa shrinkage area (the distribution of the wall area and the width of the shrinkage area L) is expanding, at this time the shell shrinkage deformation in the yield stage. When the squeeze pressure is greater than 561N (line 4), the neck shrinkage stress again appears bulge, and with the increase in squeeze pressure significantly increased. At the final stage of the loading of the ring sagittal squeeze diameter (line 6), the maximum equivalent force is 648.13Mpa concentrated in the necking squeeze area.

During unloading (lines 7-10), the overall stresses decreased continuously. At 407N (line 9), the stresses in the centre of the necking area decreased by about 400Mpa, the largest reduction, and the wall stresses at 2mm from the necking area (related to the width of the shrinkage area L=1mm) decreased slightly and remained at about 230Mpa. After complete unloading (line 10), the stresses are distributed in a triple-peaked pattern, and the stresses in the necking area show an obvious rebound increase, with the maximum residual stresses concentrated in the necking area and at a distance of 2mm from the necking area.

ISSN: 2664-9640

3.3. Analysis of stress changes in the wall thickness direction

The stresses in the necking area from the outer wall to the inner wall (wall thicknessδ=0.2mm) is shown in Figure6. Lines 1-6 are the extrusion pressure loading stage, in the early stage of extrusion (when the extrusion pressure is less than 234N), the stress along the wall thickness is basically linear growth. When the squeeze pressure is greater than 234N, the equivalent force reaches the yield limit of 255Mpa, the stress in the remaining wall thickness area is basically stable at about 255Mpa, as shown in lines 2-3. When the squeezing pressure is greater than 569N (line 4), the overall stress is distributed in a concave shape with 0.1mm (i.e. the middle of the wall thickness) as the valley.

During the unloading stage of the extrusion pressure, as shown in lines 7-12 in Figure 7, the overall stress distribution in the wall thickness direction remains concave and gradually moves downwards. In the final stage of unloading (lines 10-12), the bottom of the concave shape gradually moves towards the outer wall direction, and there is an obvious stress rebound at the wall thickness of 0.05-0.2mm.

After complete unloading, the residual stress in the wall thickness direction is basically a linear increasing distribution, the inner wall surface stress is the largest, the maximum residual stress is 202.5Mpa.

4. Experimental analysis of tube shell shrinkage

The basic principle of pipe shell reduction machine As shown in Figure 7, the work flow is: thin-walled pipe shell 6 by the transport module transported to the reduction extrusion station, fixed on the bottom plate of the hydraulic cylinder to generate thrust 2, pushing the movable plate 3 upward movement, thrust movable plate 3 in the thrust extrusion hole 4 on the upper end of the extruder 5 to generate squeezing pressure, the lower end of the extruder 5 inward.

Shrink and squeeze the thin-walled metal shell 6, the hydraulic cylinder moves downwards at the end of the extrusion work, completing the shrink forming process of the thin-walled metal shell. The results of the thin-walled tube shell ring sagittal reduction test and simulation are shown in Figure 8.As shown, the width of the neck-shrinkage extrusion zone is 1mm, and the simulation results match the neck-shrinkage shape of the thin-walled tube shell after the ring-sagittal extrusion test. The reliability of the stress model and the accuracy of the simulation results were verified.

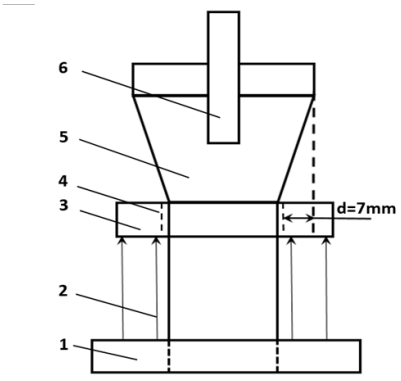

Figure 7: Schematic diagram of extrusion reducing mill

ISSN: 2664-9640

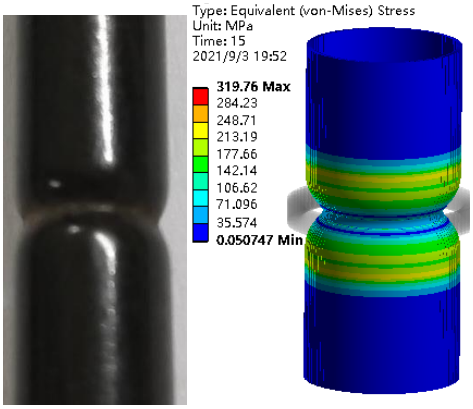

Figure 8: Comparison of experimental and simulation results

5. Conclusion

Through the theoretical analysis, numerical simulation and process tests on the ring vector reduction forming of thin-walled tube shells, the following conclusions can be drawn

(1) In the process of tube shell external compression forming, the stress on the inner wall is convex as a whole. When the maximum equivalent stress reaches the yield stress of 255mpa, the tube shell external compression deformation enters the yield stage, and the maximum equivalent stress basically remains stable, but the wall area reaching the yield stress gradually increases.

(2) The theoretical analysis of the outer shell extrusion and diameter neck shrinkage forming follows the formula (10) and (11), the thick neck ratio δ/R When the ratio remains constant, the wider the necking area L/R The smaller the necking area (if the necking area width diameter ratio L/R remains constant, the greater the thickness to neck ratio δ/R The larger the ratio, the further away from the elastic zone the necking will be; conversely, the closer to the elastic zone.

(3) The distribution of stress changes in the direction of the wall surface and wall thickness within the tube shell is related to the width of the shrinkage area and the thickness of the tube shell.

References

[1] Holmstrom,s. linder. New Technology for In-Line Control. Tube Internal.1992,49(11):219-222.

[2] Study on the Accuracy of Wall Thickness in Seamless Tube Rolling Process.Nippon Kokan Tech Rep,1985,106(2):21-30.

[3] Zhu Wei-chang.Testing and Investigation of Thin Wall Slender Tube Necking[J],Automobile Technology& Materlal, 1992(03):18-20.(in Chinese)

[4] Kubg-Keun Um,Dong Nyung.lee,An upper bound solution of tube drawing,Journal of Materials Processing Technology 63(1997)43-48.

[5] Teng Hongchun,Zhang Fenglan,Cui Bo.The Upper Limit Analysis on Precisely Reducing Diameter of Transmission Shaft Tube[J], Transacyions of The Chinese Society of Agricultural Machinery, 2000,(3): 99-101,119.(in chinese)

[6] YOSHIDA K. Purposes and features of the Yoshida wrinkling test[J].Journal of Applied Mechanics, 1999,66(3):646-652.

[7] Cao J.Prediction of Plastic Wrinkling Using the Energy Method[J]. Journal of Applied Mechanics, 1999, 66(3):236-249.

[8] JU G T,KYRIAKIDES S.Bifurcation and localization instabilities in cylindrical shells under bending-Ⅱ.Predictions J.International Journal of Solids and Structures,1992,29(9): 1143-1171.

ISSN: 2664-9640

[9] H. Li,H. Yang,M. Zhan,R.J. Gu. A new method to accurately obtain wrinkling limit diagram in NC bending process of thin-walled tube with large diameter under different loading paths[J].Journal of Materials Processing Tech.2006,177(1/3) :192-196.

[10] H. Li,H. Yang,M. Zhan .A study on plastic wrinking in thin-walled tube bending via an energy-based wrinkling prediction mode[J].Modelling and Simulation in Materials Science and Engineering,2009,17(3): 35007-35039.

[11] Reissner Hans. Discussion: "Plastic Flow as an Unstable Process" (Donnell, L. H., 1942, ASME J. Appl. Mech., 9, pp. A91–A95)[J]. J. Appl. Mech,1943,10(1):A91-A95.

[12] Nan Liu,He Yang,Heng Li,Zhijun Tao,Xiao Hu. An imperfection-based perturbation method for plastic wrinkling prediction in tube bending under multi-die constraints[J]. International Journal of Mechanical Sciences,2015,98:178-194.

[13] Chen Hui-fa.Elasticity and plasticity[M].Beijing: China Architecture & Building Press,2004.